

## RESEARCH ARTICLE

# Prediction of Fusion Rod Curvature Angles in Posterior Scoliosis Correction Using Artificial Intelligence

Rasoul Abedi, PhD; Nasser Fatouraei, PhD; Mahdi Bostanshirin, PhD; Navid Arjmand, PhD; Hasan Ghandhari, MD

Research performed at Amirkabir University of Technology, Tehran, Iran

Received: 12 December 2023

Accepted: 27 April 2024

## Abstract

**Objectives:** This study aimed to estimate post-operative rod angles in both concave and convex sides of scoliosis curvature in patients who had undergone posterior surgery, using neural networks and support vector machine (SVM) algorithms.

**Methods:** Radiographs of 72 scoliotic individuals were obtained to predict post-operative rod angles at all fusion levels (all spinal joints fused by rods). Pre-operative radiographical indices and pre-operatively resolved net joint moments of the apical vertebrae were employed as inputs for neural networks and SVM with biomechanical modeling using inverse dynamics analysis. Various group combinations were considered as inputs, based on the number of pre-operative angles and moments. Rod angles on both the concave and convex sides of the Cobb angle were considered as outputs. To assess the outcomes, root mean square errors (RMSEs) were evaluated between actual and predicted rod angles.

**Results:** Among eight groups with various combinations of radiographical and biomechanical parameters (such as Cobb, kyphosis, and lordosis, as well as joint moments), RMSEs of groups 4 (with seven radiographical angles in each case, which is greater in quantity) and 5 (with four radiographical angles and one biomechanical moment in each case, which is the least possible number of inputs with both radiographical and biomechanical parameters) were minimum, particularly in prediction of the concave rod kyphosis angle (errors were 5.5° and 6.3° for groups 4 and 5, respectively). Rod lordosis angles had larger estimation errors than rod kyphosis ones.

**Conclusion:** Neural networks and SVM can be effective techniques for the post-operative estimation of rod angles at all fusion levels to assist surgeons with rod bending procedures before actual surgery. However, since rod lordosis fusion levels vary widely across scoliosis cases, it is simpler to predict rod kyphosis angles, which is more essential for surgeons.

**Level of evidence:** IV

**Keywords:** Biomechanical modeling, Cobb angle, Neural networks, Posterior surgery, Rod kyphosis

## Introduction

There has been a growing concern over the examination of scoliosis deformities, which affect 2-4% of adolescents and affect females 10 times more often than males.<sup>1</sup> For the treatment of scoliosis in adolescents with a Cobb angle greater than 40° or 50° at bone maturation, surgical procedures are performed.<sup>2,3</sup>

One popular technique is posterior fusion surgery, which fixes and corrects vertebrae with rods. Therefore, the properties of the fixation rod, such as the material and curvature angles, which affect corrective forces and moments acting on the spine, are an important factor in accurately correcting scoliosis deformity.<sup>4,5</sup>

**Corresponding Author:** Nasser Fatouraei, Department of Biomedical Engineering, Amirkabir University of Technology, Tehran, Iran

**Email:** nasser@aut.ac.ir



THE ONLINE VERSION OF THIS ARTICLE  
ABJS.MUMS.AC.IR



Some studies have examined the impact of surgical rod contouring using biomechanical models and estimating corrective forces to examine their effects on scoliosis deformity correction in posterior surgery.<sup>4,6,7</sup> Some studies employed the modeling of scoliotic spines and rods from biplanar two-dimensional (2D) radiographs to examine rod curvatures in scoliosis surgery.<sup>8,9</sup> Furthermore, three-dimensional (3D) printed prototypes of patients' vertebrae were used for rod and screw placement as an aid in kyphoscoliosis surgery.<sup>10</sup> Nevertheless, these methods are time-consuming and have a limited number of cases for offering general outcomes.

The association between pre-operative spinal and pelvic parameters and post-operative measures, which can be used as assistance for rod curvatures, has been determined statistically in some other studies.<sup>3,11,12</sup> Some statistical studies found a relationship between post-operative Cobb and thoracic kyphosis (TK) angles and pre-operative parameters,<sup>12,13</sup> particularly with the use of pre-operative side-bending and traction radiographs.<sup>14,15</sup> A previous study also compared the effect of pre-bent, notched, and notch-free rods on scoliosis correction.<sup>16</sup> However, a particular weakness of these investigations is the absence of computing rod curvature angles at each fusion level of the spine.

Machine learning methods have also been used for the detection of scoliosis and its treatment methods in radiographs,<sup>17,18</sup> the definition of spinal fusion patterns

and the scoliosis Lenke classification,<sup>19,20</sup> quick localization and segmentation of spine vertebrae and spinal cord in patients' medical images,<sup>21-23</sup> scoliosis curve flexibility classification (structural or non-structural),<sup>24</sup> and the prediction of rod kyphosis in Lenke 5 patients following posterior scoliosis surgery.<sup>25</sup> Nevertheless, these studies did not predict all fusion levels (all spine vertebral levels fused by surgical rods and screws) of post-operative rod kyphosis and lordosis angles on both concave and convex sides.

Our prior study aimed to predict post-operative main thoracic Cobb (MTC) and TK angles in scoliosis correction surgery using the Adaptive Neuro-Fuzzy Interface System.<sup>26</sup> The purpose of this study is to estimate the post-operative concave and convex rod angles at all fusion levels in adolescent idiopathic scoliosis (AIS) patients using the combination of an artificial neural network (ANN) and support vector machine (SVM), with a number of arrangements in pre-operative clinical and biomechanical parameters of the spine. It is hypothesized that our approach provides a more accurate tool than statistical methods and yet an easier tool than developed biomechanical modeling methods to estimate post-operative concave and convex rod curvature angles for surgeons. The detailed abbreviations used in this study are listed and described in [Table 1].

**Table 1. Description of abbreviations used in the study**

Abbreviation	Definition
ANN	Artificial neural networks
SVM	Support vector machine
PTC	Proximal thoracic Cobb
MTC	Main thoracic Cobb
TLC	Thoracolumbar Cobb
PI	Pelvic incidence
TK	Thoracic kyphosis
LL	Lumbar lordosis
T1SPi	T1-SpinoPelvic inclination
Mfe	Moment of spine flexion/extension
Mlb	Moment of spine lateral bending
Mar	Moment of spine axial rotation
RMSE	Root mean square error
RKcc	Rod kyphosis on the concave side
RKcv	Rod kyphosis on the convex side
RLcc	Rod lordosis on the concave side
RLcv	Rod lordosis on the convex side

## Materials and Methods

This is a retrospective study using radiographical and biomechanical parameters and machine learning methods to estimate post-operative rod curvature angles at all estimated

fusion levels of posterior scoliosis correction surgery.

### Collection and Analysis of Patients' Radiographs

The biplanar EOS imaging system, which has the ability to perform low-dose radiography in both frontal and sagittal

views,<sup>27,28</sup> was used to collect pre- and post-operative radiographs of 72 scoliotic patients (12 males and 60 females) of different Lenke types with lumbar modifiers A, B, and C at the ages of 17±4 years who received posterior scoliosis correction surgery from spine surgery specialists. Overall, 49 patients were Lenke A (with a mean MTC angle of 62.0°), and the other 23 were Lenke B and C (with a mean thoracolumbar Cobb [TLC] angle of 49.4°).

Ethical approval was received from the Ethics Committee for receiving and performing analysis on scoliotic patients' EOS radiographs under letter No. IR.IUMS.REC.1398.1162, dated 02/22/2020. Therefore, the standards laid down in the Declaration of Helsinki have been adhered to. Informed consent was also obtained from all patients.

Pre-operative radiographical indices were measured in EOS radiographs using Surgimap (version 2.3.2.1, Nemaris Inc., New York, USA), including proximal thoracic Cobb (PTC), MTC, TLC, TK from T1 to T12, lumbar lordosis from L1 to S1, pelvic incidence, and T1 spinopelvic inclination (T1SPi) angles [Figure 1a]. Moreover, rod kyphosis and lordosis angles were calculated by measuring concave and convex rod angles (in rods with a circular diameter of 5.5 mm) at all fusion levels using post-operative radiographs. In Surgimap, rod and line tools were used to measure rod angles at each fusion level between pedicle screws. To identify concave and convex sides in the rods, the frontal view of post-operative images was examined in addition to their sagittal view. In fact, the combination of both views helped to identify concave and convex rods, as illustrated in [Figures 1c and 1d]. Due to the coincidence of concave and convex rod contours in the sagittal view of post-operative scoliosis radiographs, the convex side contour was transferred manually in Figure 1c to illustrate both sides separately.

### Biomechanical Modeling and Analysis

The OpenSim software (version 4.4, SimTK, Stanford, USA) was used to generate scoliosis deformity models based on

biplanar radiographs using a developed thoracolumbar spine model. In fact, the model contained every intervertebral joint from T1-T2 to L5-S1 level, with three degrees of freedom for each level, including flexion/extension (Mfe), lateral bending (M1b), and axial rotation (Mar).<sup>29,30</sup>

Surgimap was used to quantify pre-operative vertebral angles from T1 to S1 levels in frontal and sagittal radiographs, and these measurements were then applied to the OpenSim model as an input motion file. The motion file contained all vertebral angles from T1 to S1, including T1-T2 to L5-S1 Mfe, M1b, and Mar. As can be seen in Figure 1b, the local coordinate system of each vertebral joint (based on anatomical axes) was used to calculate vertebral angles. Thereafter, vertebral net joint moments, including Mfe, M1b, and Mar moments, were calculated using inverse dynamic analysis. This analysis calculates net moments from external moments (moments due to weights of the upper body above vertebrae) with static equilibrium of moments. Specifically, the net moment of the apical vertebral joint was used for the neural network analysis [Figure 1b]. The following equation is an example of moment calculation in the apical vertebral joint:

$$\text{apical joint moment} = \sum_{i=1}^N L_i m_i g \sin \theta_i + M_{\text{ext\_load}}$$

Where N is the total number of spinal joint levels above the apical vertebrae, m is the mass of each spinal level, which is calculated based on anthropometry data of the total body mass of the case in OpenSim software, L is the distance from the vertebral center of the mass to its lower spinal joint, g is the gravity acceleration, and  $\theta$  is the vertebral angle with respect to the horizontal axis, which is measured in patients' radiographs in Surgimap software. In addition,  $M_{\text{ext\_load}}$  is the external moment due to the external weights of other body parts, such as the head, shoulders, or other parts, which is calculated in OpenSim using anthropometry data of the case.

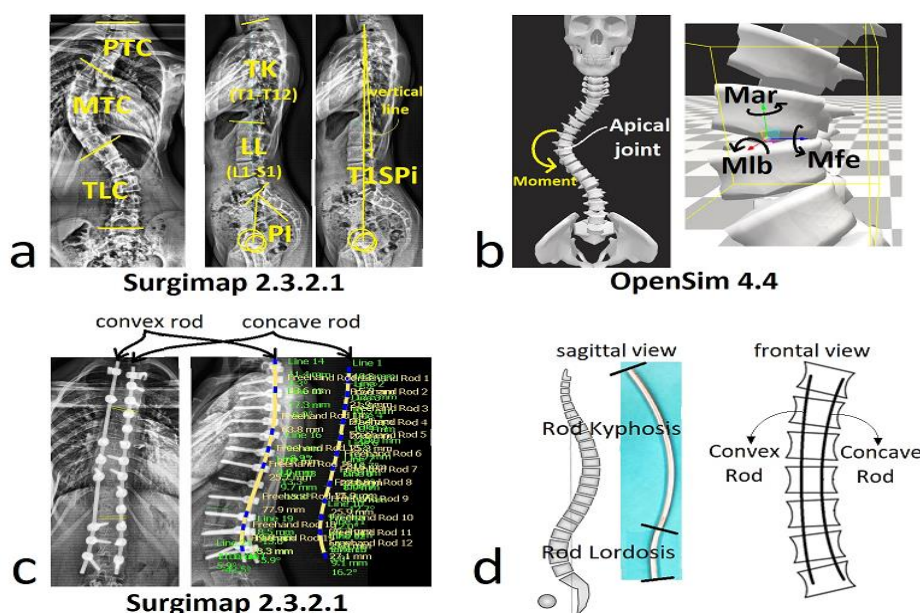


Figure 1. a. Pre-operative radiographic indices, b. Net moments of the apical vertebral joint, c. Post-operative, level-by-level rod curvature angles, and d. Schematic of concave and convex rods with illustration of rod kyphosis and lordosis angles

### Combining Neural Network and Support Vector Machine Estimations

An ANN was trained and tested on pre- and post-operative datasets to predict post-operative concave and convex rod curvatures at all fusion levels. The ANN inputs included pre-operative parameters (namely, PTC, MTC, TLC, PI, TK, LL, T1SPi, Mfe, Mlb, and Mar), and the outputs included rod curvature angles at 34 spinal levels from T1 to S1 (17 levels for the concave and 17 levels for the convex side). The estimation errors were calculated with one or two hidden layers in addition to ANN input and output layers, with a different number of neurons (error calculation using trial-and-error with a different combination of hidden layers). During the trial-and-error procedure, the root mean square error (RMSE) was at its minimum in the situation with five neurons in the first layer and 15 neurons in the second layer. It might be due to the number of ANN outputs (34 spinal joint levels, 17 for the concave and 17 for the convex side) that the second hidden layer had more neurons than the first one. The activation function of neurons was defined as their sigmoid

function. To distinguish rod angles in ANN outputs, rod kyphosis and lordosis angles were assumed to have positive and negative values, respectively.

The diagnosis of upper and lower fusion levels of concave and convex rods was performed using SVM with a kernel of type radial basis function (RBF). The RBF kernel is a popular choice due to its flexibility in modeling complex, non-linear relationships in data. Moreover, its construction is similar to that of a normal (gaussian) distribution, which is common in data distribution analysis.

ANN and SVM inputs were equivalent in pre-operative parameters, such as PTC, MTC, TLC, PI, TK, LL, T1SPi, Mlb, MFe and Mar. There were two values in SVM outputs: 0 represented the spinal level that was not fused, and 1 represented the fused level. SVM was evaluated and trained to identify all fused levels for each spinal level, and thus the upper and lower fusion levels of concave and convex rods could subsequently be anticipated. The flowchart of the ANN+SVM algorithm can be seen in [Figure 2].

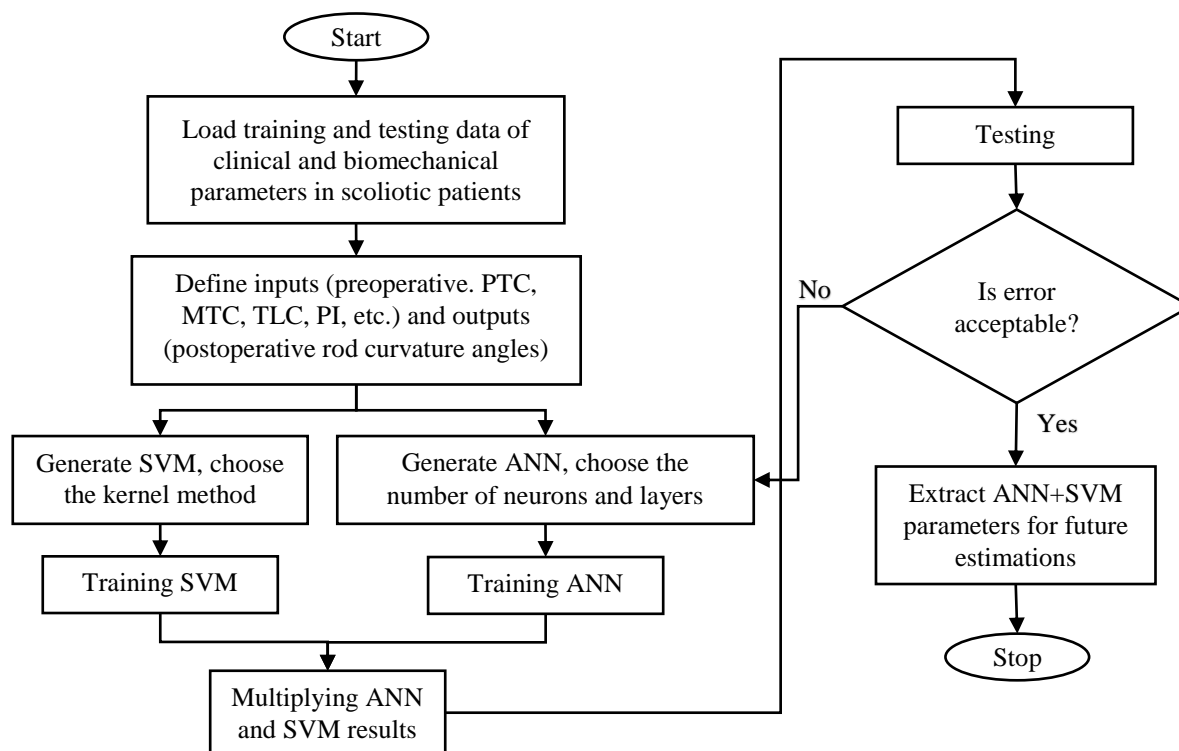


Figure 2. Flowchart of the ANN+SVM structure for estimating post-operative rod curvature angles

The percentage of train and test data was taken into account for both ANN and SVM analyses at 85% and 15%, respectively. Most of the dataset is used to train the network, and a part of it is used to test the network and figure out how it can predict outputs for new inputs that are not used in training it. In this study, because of the limited number of

cases, 85% of the dataset (pre-operative scoliosis parameters and post-operative rod angles) was used to train neural networks, and 15% was used to test it. In a larger number of cases, this proportion can change to 80%-20%, 75%-25%, or 70%-30%.

ANN might predict rod angle values for spinal levels that do

not necessarily need to be fused by the rod. SVM predicts fused and unfused levels as values 1 and 0, respectively. Therefore, to estimate rod angles at the anticipated fusion predicted values of rod curvatures in both kyphosis and lordosis angles can thus be used to quantify estimation errors. Rod angles and RMSE are defined as follows:

$$RK_{cc} = \sum_i \theta_{k-cc}(i), RL_{cc} = \sum_i \theta_{l-cc}(i), RK_{cv} = \sum_i \theta_{k-cv}(i), RL_{cv} = \sum_i \theta_{l-cv}(i)$$

$$RMSE_{RA} = \sqrt{\frac{1}{n} \sum_{i=1}^n (Actual\_RA_i - Predicted\_RA_i)^2}$$

Where  $\theta_k$  and  $\theta_L$  represent rod kyphosis and lordosis angles at each fusion level, respectively, cc and cv are related to the concave and convex sides, respectively. The total rod kyphosis angle on both sides (RKcc and RKcv for concave and convex, respectively) was calculated as the sum of  $\theta_k$  angles at all kyphosis levels. Similarly, the total rod lordosis angle on

levels, the results of ANN and SVM were multiplied together to remove predictions of ANN for unfused levels when multiplied by zero. The differences between the actual and both sides (RKcc and RKcv) was calculated as the sum of  $\theta_L$  angles at all lordosis levels. Subsequently, the RMSE of total rod angles (RMSE<sub>RA</sub>) was defined between actual and predicted angles in both rod kyphosis and lordosis. Moreover, n represents the number of scoliotic cases considered in the error calculation (10 cases for the test).

Different arrangements of pre-operative parameters in eight groups were considered as inputs for both ANN and SVM [Table 2]. The 34 outputs (17 levels for the concave and 17 for the convex side) were  $\theta_{k-cc}$ ,  $\theta_{l-cc}$ ,  $\theta_{k-cv}$ , and  $\theta_{l-cv}$  angles, where  $\theta_k$  angles were assumed to be positive and  $\theta_L$  angles were assumed to be negative values to distinguish between estimating rod kyphosis and lordosis angles. Figure 3 illustrates the parameters of rod angles on concave and convex sides used in the formulae mentioned [Figure 3].

Table 2. Classification of pre-operative parameters as ANN+SVM inputs in eight groups		
Group number	Description	ANN+SVM inputs (pre-operative clinical indices)
Group 1	Four radiographical angles	MTC, PI, TK, and T1SPi
Group 2	Five radiographical angles	MTC, PI, TK, LL, and T1SPi
Group 3	Six radiographical angles	PTC, MTC, TLC, PI, TK, and T1SPi
Group 4	Seven radiographical angles	PTC, MTC, TLC, PI, TK, LL, and T1SPi
Group 5	Four radiographical angles + One biomechanical moment	MTC, PI, TK, T1SPi, and Mlb
Group 6	Five radiographical angles + One biomechanical moment	MTC, PI, TK, LL, T1SPi, and Mlb
Group 7	Five radiographical angles + Two biomechanical moments	MTC, PI, TK, LL, T1SPi, Mfe, and Mlb
Group 8	Five radiographical angles + Three biomechanical moments	MTC, PI, TK, T1SPi, Mfe, Mlb, and Mar

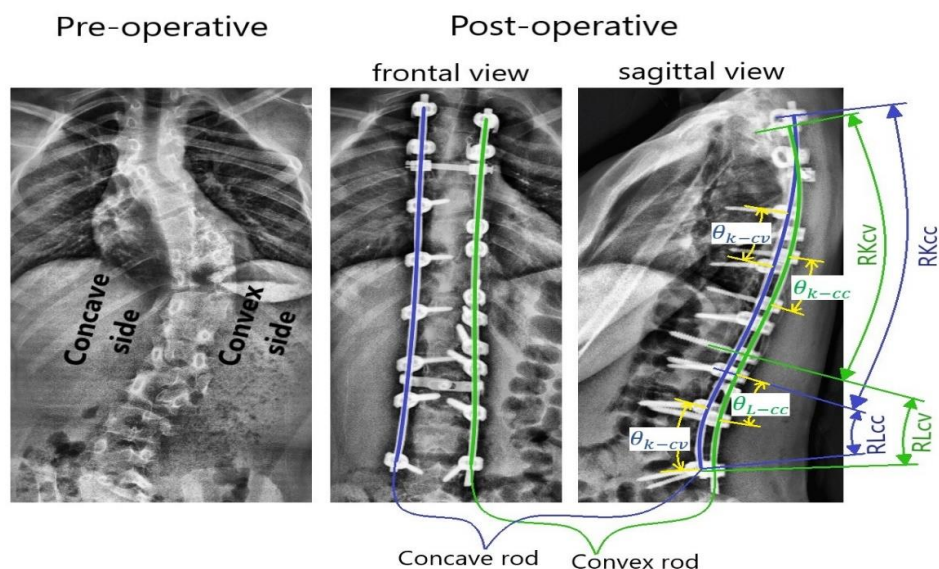


Figure 3. Visual representation of the concept of rod angles on concave and convex sides: RKcc (rod kyphosis in concave side), RKcv (rod kyphosis in convex side), RLcc (rod lordosis in concave side), and RLcv (rod lordosis in convex side),  $\theta_{k-cc}$  (rod kyphosis angle in concave side for one fusion level),  $\theta_{k-cv}$  (rod kyphosis angle in convex side for one fusion level),  $\theta_{l-cc}$  (rod lordosis angle in concave side for one fusion level), and  $\theta_{l-cv}$  (rod lordosis angle in convex side for one fusion level)

### Results

#### RMSE Values in Estimating Rod Angles

In most groups, the RMSE values of rod lordosis angles (RLcc and RLcv for concave and convex, respectively) were higher than those of kyphosis angles (RKcc and RKcv). Nevertheless, when Lenke A cases were examined, the RMSE of rod lordosis became lower than that of other Lenke types. Moreover, in most groups, the RMSE of RKcc was higher than that of RKcv. Groups 4 and 5 of all Lenke types and groups 7 and 8 of Lenke A cases had the lowest RMSE in RKcc, as illustrated in [Figures 4a and 4b]. RKcc is usually more important than RKcv for surgeons, as they usually attempt to correct scoliosis deformity by applying concave rod kyphosis

at first.

Overall, 10 test cases (15% of the total 72) from groups 4 and 5 were specifically evaluated as samples of the lowest RMSE in RKcc prediction. In the majority of test cases, the RMSE of RKcc was lower than that of RKcv, and the RMSE of rod kyphosis was lower than that of lordosis, as illustrated in [Figures 4c and 4d]. Test cases 1 and 2 in group 4 and test cases 8 and 10 in group 5 were chosen as two sample cases from each group for additional rod curvature analysis (two cases with an almost lower and higher RMSE in each group).

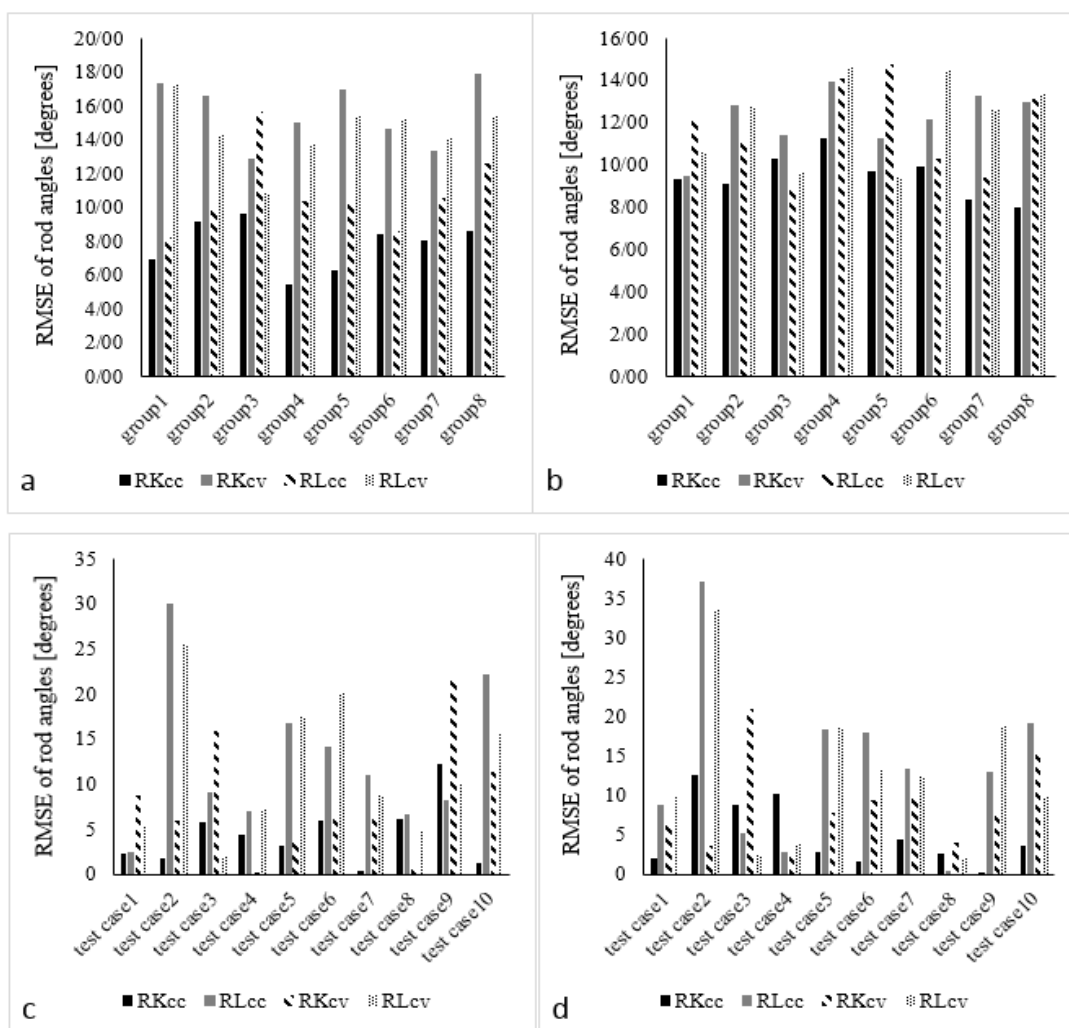


Figure 4. RMSE values for post-operative rod angle estimations (RKcc, RKcv, RLcc, and RLcv), a. for all Lenke type cases in eight groups, b. for Lenke A cases in eight groups, c. for test cases in group 4, and d. for test cases in group 5

#### Prediction of Post-Operative Rod Curvature Angles

Test cases 1 and 2 in group 4 were of Lenke A and C types, respectively. The actual and predicted concave and convex rod curvatures in these cases are depicted in [Figure 5]. The

values of actual and predicted rod level angles (positive for rod kyphosis and negative for rod lordosis) are also shown in [Table 3].

**Table 3. Comparison of actual and predicted values of the concave and convex rod angles at different spinal levels in two test cases in group 4**

Spinal levels	Test case 1 from group 4				Test case 2 from group 4			
	Concave-predicted angle (degrees)	Convex-predicted angle (degrees)	Concave-actual angle (degrees)	Convex-actual angle (degrees)	Concave-predicted angle (degrees)	Convex-predicted angle (degrees)	Concave-actual angle (degrees)	Convex-actual angle (degrees)
<i>T1-T2</i>	-	-	-	-	-	-	-	-
<i>T2-T3</i>	2.7	2.5	-	-	4.5	2.5	-	-
<i>T3-T4</i>	4.1	3.5	-	-	4.8	4.7	8.1	4.4
<i>T4-T5</i>	3.1	4.6	3.3	1.8	3.9	6.2	0.5	7.4
<i>T5-T6</i>	3.8	3.8	1.3	3.5	3.6	4.6	1.5	4.1
<i>T6-T7</i>	3.5	4.1	2.9	2.7	5.1	6.3	3.6	3.8
<i>T7-T8</i>	2.9	4.5	2.7	3.1	5.3	6.8	8.2	3.5
<i>T8-T9</i>	1.7	2.6	1.9	3.8	4.0	3.5	5.8	-1.1
<i>T9-T10</i>	0.7	2.2	2.3	4.4	3.1	3.4	4.1	1.6
<i>T10-T11</i>	0.0	1.9	3.2	2.7	0.9	1.0	3.1	3.4
<i>T11-T12</i>	-1.4	-0.5	-2.7	-2.7	-1.5	1.4	-1.0	2.5
<i>T12-L1</i>	-3.4	-3.2	-8.6	-8.2	-0.5	-1.1	-5.8	-2.5
<i>L1-L2</i>	-4.8	-2.4	-	-	-5.4	-7.1	-11.2	-6.6
<i>L2-L3</i>	-3.5	-1.9	-	-	-7.7	-8.2	-15.9	-7.5
<i>L3-L4</i>	-	-	-	-	-	-	-9.0	-9.7
<i>L4-L5</i>	-	-	-	-	-	-	-	-
<i>L5-S1</i>	-	-	-	-	-	-	-	-
<b>Total rod kyphosis (degrees)</b>	22.5	29.6	17.6	22.0	35.0	40.5	34.9	31.8
<b>Total rod lordosis (degrees)</b>	-13.2	-8.0	-11.3	-10.9	-15.2	-16.5	-42.9	-26.3

Lenke 1A, which is nearly S-shaped, and Lenke 2A, which is nearly C-shaped, were test cases 8 and 10 in group 5, respectively. The actual and predicted concave and convex rod curvatures of these cases are illustrated in Figure 6, with their fusion level angles in [Figure 6, Table 4]. The description of all test cases is presented in [Table 5].

Generally, by comparing rod curvatures in Figures 5 and 6, decreasing or increasing rod kyphosis or lordosis angles almost follow identical trends between actual and predicted rods. However, some areas, such as first or last fusion levels and rod lordosis angles, demonstrate some differences, as indicated in [Tables 3 and 4]. The total rod kyphosis and lordosis angles for the four test cases, along with actual and predicted values, are presented in the last two rows of Tables 3 and 4, respectively, which further indicates that the differences in actual and predicted values of total rod angles in the four test cases are more obvious in rod lordosis regions. Kyphosis angles are considered positive, and lordosis angles are considered negative; therefore, the summation of positive angles in each column equals the total rod kyphosis (in the row before the last), and the summation

of negative angles equals the total rod lordosis (in the last row).

## Discussion

### Analysis of the Results

The estimation of rod kyphosis angles is very important and helpful for surgeons<sup>16</sup> since they usually attempt to fix the thoracic Cobb angle and turn it into TK if possible, which would be conceivable by the rod kyphosis angle. As a result, rod lordosis is more changeable across different cases, and estimation errors would be greater in lordosis regions. Moreover, RKcc is a critical rod angle since surgeons usually attempt to fix the patient's TK by rod kyphosis of the concave side at first and then stabilize it with the convex rod.<sup>7,31,32</sup> The RMSE of test data for RKcc was almost the lowest in groups 4 and 5 of all Lenke types Figures 4a and 4b, which can be due to the effect of considering more pre-operative radiographical indices of the scoliotic spine in group 4 and the M1b moment effect in group 5.

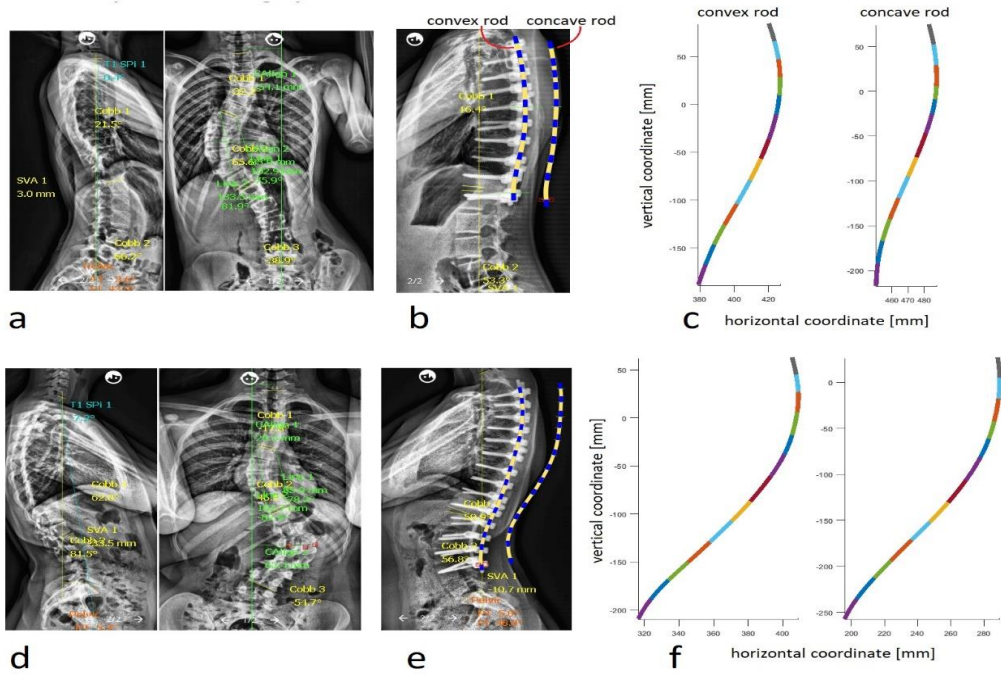


Figure 5. Illustration of a. pre-operative radiographs, b. actual rod curvatures, and c. predicted rod curvatures for test case 1 in group 4. Similarly, d, e, and f. for test case 2 in group 4

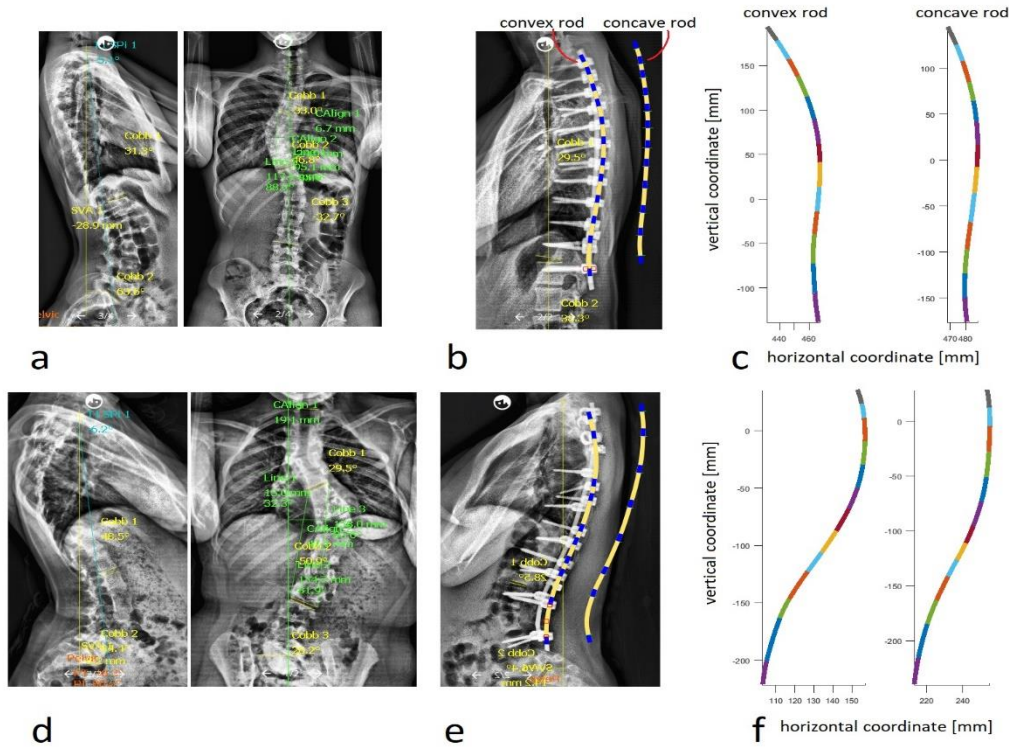


Figure 6. Illustration of a. pre-operative radiographs, b. actual rod curvatures, and c. predicted rod curvatures for test case 8 in group 5. Similarly, d, e, and f. for test case 10 in group 5

Table 4. Comparison of actual and predicted values of the concave and convex rod angles at different spinal levels in two test cases in group 5

Spinal levels	Test case 8 from group 5				Test case 10 from group 5			
	Concave-predicted angle (degrees)	Convex-predicted angle (degrees)	Concave-actual angle (degrees)	Convex-actual angle (degrees)	Concave-predicted angle (degrees)	Convex-predicted angle (degrees)	Concave-actual angle (degrees)	Convex-actual angle (degrees)
T1-T2	-	-	-	-	-	-	-	-
T2-T3	2.4	2.1	9.4	9	3.7	4.6	4.3	2.9
T3-T4	3.0	2.6	0.1	1.1	3.3	5.0	4.0	3.2
T4-T5	2.3	2.8	1	1.8	1.2	4.0	4.2	5.0
T5-T6	2.6	3.5	4.7	6.9	2.8	4.5	3.8	5.1
T6-T7	3.4	4.1	2.6	5.3	4.6	5.7	2.9	5.2
T7-T8	3.4	5.2	2.4	5.6	3.8	5.9	2.6	4.7
T8-T9	2.4	3.2	0.2	2	3.3	3.9	1.5	3.0
T9-T10	1.9	2.8	0.6	0.4	2.2	2.8	1.5	2.6
T10-T11	0.7	2.0	2.3	1.8	-1.6	0.5	1.4	-0.1
T11-T12	-0.7	-0.5	-3.2	-4.5	-1.8	-4.0	1.6	-0.8
T12-L1	-2.4	-4.8	-7.6	-9.3	-4.3	-7.2	1.4	-0.4
L1-L2	-2.9	-1.4	-	-	-4.0	-4.6	-6.1	-8.8
L2-L3	-3.5	-3.2	-	-	-3.4	-4.9	-13.1	-6.3
L3-L4	-	-	-	-	-	-	-13.5	-6.5
L4-L5	-	-	-	-	-	-	-	-
L5-S1	-	-	-	-	-	-	-	-
Total rod kyphosis (degrees)	22.0	29.6	17.6	22.0	25.0	36.8	34.9	31.6
Total rod lordosis (degrees)	-9.6	-9.9	-11.3	-10.9	-15.1	-20.8	-32.6	-22.8

Table 5. Description of test cases

Test case number	Group number	Group inputs	Lenke type and deformity description	deformity schematic
1	4	PTC, MTC, TLC, PI, TK, LL, T1SPi	Lenke A, with a greater thoracic Cobb angle	
2	4	PTC, MTC, TLC, PI, TK, LL, T1SPi	Lenke C, with a greater lumbar Cobb angle	
8	5	MTC, PI, TK, T1SPi, Mlb	Lenke A, S-shaped curve	
10	5	MTC, PI, TK, T1SPi, Mlb	Lenke A, C-shaped curve	

In the test cases of Lenke A type, the RMSE of the test data in RLcc and RLcv exhibited smaller values compared to other Lenke types. This observation can be attributed to the accurate estimation of rod lordosis angles, which demonstrates similar patterns in scoliosis cases classified as Lenke A. This is because Lenke types B and C have greater values of the Cobb angle in the lumbar part, and rod lordosis angles with different fusion levels vary widely across different Lenke types. In addition, the RMSE of RKcc was almost the lowest in groups 7 and 8 in the test data of Lenke A type. This improvement can be attributed to the incorporation of pre-operative radiographical indices and net joint moments of the apical vertebrae in these groups. Notably, the net moments generated by internal tissues at spinal joints, such as muscles, can have a substantial impact on scoliosis correction and the curvatures of the rods.<sup>33</sup>

According to Figure 5, since surgeons usually correct the deformity using kyphosis of the first rod on the concave side, it can help the RKcc have a lower RMSE than the RKcv in most test cases. Furthermore, because of the greater variations in rod lordosis angles and fusion levels, it may cause the rod lordosis angles (RLcc and RLcv) to have greater RMSE values than the kyphosis ones (RKcc and RKcv) in most test cases, which has been mentioned in some previous studies.<sup>25,32</sup>

Test case 1 in group 4 was Lenke A, and test case 2 was Lenke C [Figure 5 and Table 3]. Due to the large number of Lenke A cases (49 out of 72), it was more difficult for ANN+SVM to predict rod curvature angles for Lenke C. Therefore, the RMSE was greater and created more differences between actual and predicted rod curvatures. Furthermore, as can be seen in Figure 6 and Table 4, test case 10 in group 5 has a long C-shaped Cobb angle, while test case 8 is S-shaped and is more frequent in the 72 cases. Therefore, it was more difficult for ANN+SVM to predict rod curvature for a C-shaped one (especially in the rod lordosis region).

As indicated in Tables 3 and 4, it can be concluded that there are more differences between actual and predicted rod angles in regions that have more variations across different scoliotic patients, including upper and lower fusion levels, the level at which rod kyphosis turns into lordosis, and lordosis regions.

### Limitations

This study was conducted on a limited number of cases, and thus more cases may improve the prediction of post-operative rod curvatures. In addition, different types of scoliosis curves (Lenke A, B, and C, as well as hypo- or hyper-kyphosis) were collected together for ANN+SVM estimations due to the limited number of cases. Spinal joint stiffness could have affected the amount of scoliosis curve correction and rod curvatures, which was not considered in this study. Moreover, there could be some errors because of 2D radiograph measurements in radiographical indices and joint moments, while scoliosis is a 3D deformity that affects the measurements, amount of correction, and rod curvatures.<sup>34,35</sup> Nevertheless, we did not have access to 3D spine geometries. Therefore, surgical techniques such as translation, compression, distraction, and de-rotation, which

affect the 3D deformity of scoliosis, could not be analyzed. These limitations can thus be considered for development in future work.

### Conclusion

The ANN+SVM machine learning algorithm is a robust method for predicting post-operative rod curvature angles and fusion levels in scoliosis patients. This algorithm has the potential to serve as an assistive tool for surgeons, allowing them to bend surgical rods prior to the actual operation and thereby reduce the duration of surgery. In this process, a pre-operative AIS radiograph is obtained and analyzed using radiographical indices, such as PTC, MTC, TLC, PI, TK, LL and T1SPi. These indices are then used as inputs for a trained ANN+SVM network, which predicts the post-operative rod curvature angles. The entire process can be completed within a few minutes, providing the surgeon with a report of the predicted results prior to surgery. It is also worth mentioning that this rod curvature prediction method is applicable even for non-experienced surgeons, as it is based on neural networks that have been trained using data analyzed by professionals and spine specialists. In other words, the surgeon takes patients' radiographs, measures pre-operative angles, and then enters angle values in the application designed based on ANN+SVM in scoliosis dataset analysis. Finally, the surgeon receives predicted post-operative rod angles and fusion levels, which can be used as a rapid guide for the actual surgery. To conclude, our initial hypothesis in the introduction section was that ANN+SVM can provide a more accurate tool than statistical methods, which is yet an easier tool than developed biomechanical modeling methods to estimate postoperative concave and convex rod curvature angles for surgeons, which can potentially be corroborated by reality.

### Acknowledgement

The study was supported by Iran University of Medical Sciences, which facilitated the acquisition of EOS radiographs of AIS patients from Shafa Yahyaian Hospital.

### Authors Contribution:

Abedi contributed to data analysis, programming, and manuscript writing. He also collected and investigated the required data of patients' radiographs. Ghandhari acted as the consultant in the medical aspects of the project such as scoliosis surgery procedure and analysis of patients' radiographs. Arjmand acted as a consultant in the artificial intelligence method used for this study and revising the manuscript. And Fatourae and Bostanshirin supervised/co-supervised the project through protocol development and manuscript editing. All authors read and approved the final manuscript.

**Declaration of Conflict of Interest:** There no conflicts of interest for the authors to declare

**Declaration of Funding:** The authors did not receive any financial support for the preparation, investigation, authorship, and publication of this manuscript.

**Declaration of Ethical Approval for Study:** The ethical approval was obtained from the Ethics Committee of the Iran University of Medical Sciences (IUMS) for analyzing scoliotic patients' EOS radiographs under letter no. IR.IUMS.REC.1398.1162, dated 02/22/2020. Therefore, the standards laid down in the Declaration of Helsinki have been adhered to in this research.

**Declaration of Informed Consent:** This manuscript contains no information (e.g., names, initials, hospital identification numbers, or photographs) through which patients could be identified.

Rasoul Abedi PhD<sup>1</sup>  
Nasser Fatouraei PhD<sup>1</sup>  
Mahdi Bostanshirin PhD<sup>1</sup>  
Navid Arjmand PhD<sup>2</sup>  
Hasan Ghandhari MD<sup>3</sup>

1 Department of Biomedical Engineering, Amirkabir University of Technology, Tehran, Iran

2 Department of Mechanical Engineering, Sharif University of Technology, Tehran, Iran

3 Bone and Joint Reconstruction Research Center, Shafa Orthopedic Hospital, Iran University of Medical Sciences, Tehran, Iran.

## References

- Sharifmoradi K, Naderi A, Saljoghian P. The Effect of Boston Brace on Lower Limb and L5-S1 Joint Contact Forces during Walking in Patients with Idiopathic Scoliosis. *Scientific journal of Ilam University of medical sciences*. 2017; 25(3):90-99.
- Luković V, Čuković S, Milošević D, Devedžić G. An ontology-based module of the information system ScolioMedIS for 3D digital diagnosis of adolescent scoliosis. *Comput Methods Programs Biomed*. 2019;178:247-263. doi: 10.1016/j.cmpb.2019.06.027.
- Arima H, Hasegawa T, Yamato Y, et al. Clinical Outcomes and Complications of Corrective Fusion Surgery Down to L4, L5, and the Pelvis for Adult Scoliosis in Patients Younger than 50 Years. *Spine Surg Relat Res*. 2022; 6(5):518-525. doi: 10.22603/ssrr.2021-0220.
- Salmingo RA, Tadano S, Fujisaki K, Abe Y, Ito M. Relationship of forces acting on implant rods and degree of scoliosis correction. *Clin Biomech (Bristol, Avon)*. 2013; 28(2):122-8. doi: 10.1016/j.clinbiomech.2012.12.001.
- Yang JH, Suh SW, Chang D-G. Comparison of surgical correction rates between titanium and cobalt-chrome-alloy as rod materials in adolescent idiopathic scoliosis. *Sci Rep*. 2020; 10(1):10053. doi: 10.1038/s41598-020-66975-x.
- Wang W, Baran GR, Betz RR, Samdani AF, Pahys JM, Cahill PJ. The use of finite element models to assist understanding and treatment for scoliosis: a review paper. *Spine Deform*. 2014; 2(1):10-27. doi: 10.1016/j.jspd.2013.09.007.
- Salmingo RA, Tadano S, Abe Y, Ito M. Influence of implant rod curvature on sagittal correction of scoliosis deformity. *Spine J*. 2014; 14(8):1432-9. doi: 10.1016/j.spinee.2013.08.042.
- Le Navéaux F, Aubin C-E, Parent S, O Newton P, Labelle H. 3D rod shape changes in adolescent idiopathic scoliosis instrumentation: how much does it impact correction? *Eur Spine J*. 2017; 26(6):1676-1683. doi: 10.1007/s00586-017-4958-1.
- Courvoisier A, Cebrian A, Simon J, et al. Virtual Scoliosis Surgery Using a 3D-Printed Model Based on Biplanar Radiographs. *Bioengineering (Basel)*. 2022; 9(9):469. doi: 10.3390/bioengineering9090469.
- Shah K, Gadiya A, Shah M, et al. Does Three-dimensional printed patient-specific templates add benefit in revision surgeries for complex pediatric kyphoscoliosis deformity with sublaminar wires in situ? A clinical study. *Asian Spine J*. 2021; 15(1):46-53. doi: 10.31616/asj.2019.0021.
- Ghandhari H, Mahabadi MA, Nikouei F, et al. The role of spinopelvic parameters in clinical outcomes of spinal osteotomies in patients with sagittal imbalance. *Arch Bone Jt Surg*. 2018; 6(4):324-330.
- Solla F, Ilharreborde B, Blondel B, et al. Can Lumbopelvic Parameters Be Used to Predict Thoracic Kyphosis at all Ages? A National Cross-Sectional Study. *Global Spine J*. 2024; 14(4):1116-1124. doi: 10.1177/21925682221134039.
- Hu B, Wang L, Song Y, Yang X, Liu L, Zhou C. Postoperative proximal junctional kyphosis correlated with thoracic inlet angle in Lenke 5c adolescent idiopathic scoliosis patients following posterior surgery. *BMC Musculoskelet Disord*. 2022; 23(1):919. doi: 10.1186/s12891-022-05868-8.
- Junaid J. Prediction of Scoliosis Curve Correction Using Apical Fulcrum Bending Radiographs in Adolescent Idiopathic Scoliosis (AIS). *Pakistan Journal of Medicine and Dentistry*. 2021; 10(3):47-53.
- Tokala DP, Nelson IW, Mehta JS, Powell R, Grannum S, Hutchinson MJ. Prediction of scoliosis curve correction using pedicle screw constructs in AIS: A comparison of fulcrum bend radiographs and traction radiographs under general anesthesia. *Global Spine J*. 2018 (7):676-682. doi: 10.1177/2192568218763147.
- Sudo H, Tachi H, Kokabu T, et al. In vivo deformation of anatomically pre-bent rods in thoracic adolescent idiopathic scoliosis. *Sci Rep*. 2021; 11(1):12622. doi: 10.1038/s41598-021-92187-y.
- Kokabu T, Kanai S, Kawakami N, et al. An algorithm for using deep learning convolutional neural networks with three dimensional depth sensor imaging in scoliosis detection. *Spine J*. 2021; 21(6):980-987. doi: 10.1016/j.spinee.2021.01.022.
- Vergari C, Skalli W, Gajny L. A convolutional neural network to detect scoliosis treatment in radiographs. *Int J Comput Assist Radiol Surg*. 2020; 15(6):1069-1074. doi: 10.1007/s11548-020-02173-4.

19. Phan P, Mezghani N, Wai EK, de Guise J, Labelle H. Artificial neural networks assessing adolescent idiopathic scoliosis: comparison with Lenke classification. *Spine J.* 2013; 13(11):1527-33. doi: 10.1016/j.spinee.2013.07.449.
20. Mezghani N, Phan P, Mitiche A, Labelle H, De Guise JA. A Kohonen neural network description of scoliosis fused regions and their corresponding Lenke classification. *Int J*
22. Nozawa K, Maki S, Furuya T, et al. Magnetic resonance image segmentation of the compressed spinal cord in patients with degenerative cervical myelopathy using convolutional neural networks. *Int J Comput Assist Radiol Surg.* 2023; 18(1):45-54. doi: 10.1007/s11548-022-02783-0.
23. Galbusera F, Casaroli G, Bassani T. Artificial intelligence and machine learning in spine research. *JOR Spine.* 2019; 2(1):e1044. doi: 10.1002/jsp2.1044.
24. Yang D, Lee T, Lai K, et al. Semi-automatic method for pre-surgery scoliosis classification on X-ray images using Bending Asymmetry Index. *Int J Comput Assist Radiol Surg.* 2022; 17(12):2239-2251. doi: 10.1007/s11548-022-02740-x.
25. Peng L, Lan L, Xiu P, et al. Prediction of proximal junctional kyphosis after posterior scoliosis surgery with machine learning in the Lenke 5 adolescent idiopathic scoliosis patient. *Front Bioeng Biotechnol.* 2020;8:559387. doi: 10.3389/fbioe.2020.559387.
26. Abedi R, Fatouraee N, Bostanshirin M, Arjmand N, Ghandhari H. Prediction of Post-operative Clinical Indices in Scoliosis Correction Surgery Using an Adaptive Neuro-fuzzy Interface System. *Arch Bone Jt Surg.* 2023; 11(4):241-247. doi: 10.22038/ABJS.2022.66559.3176.
27. Garg B, Mehta N, Bansal T, Malhotra R. EOS® imaging: Concept and current applications in spinal disorders. *J Clin Orthop Trauma.* 2020; 11(5):786-793. doi: 10.1016/j.jcot.2020.06.012.
28. Melhem E, Assi A, El Rachkidi R, Ghanem I. EOS® biplanar X-ray imaging: concept, developments, benefits, and limitations. *J Child Orthop.* 2016; 10(1):1-14. doi: 10.1007/s11832-016-0713-0.
29. Schmid S, Burkhart KA, Allaire BT, Grindle D, Anderson DE. Musculoskeletal full-body models including a detailed Comput Assist Radiol Surg. 2012;7(2):257-64. doi: 10.1007/s11548-011-0667-0.
21. Rak M, Steffen J, Meyer A, Hansen C, Tönnies KD. Combining convolutional neural networks and star convex cuts for fast whole spine vertebra segmentation in MRI. *Comput Methods Programs Biomed.* 2019;177:47-56. doi: 10.1016/j.cmpb.2019.05.003.
- thoracolumbar spine for children and adolescents aged 6–18 years. *J Biomech.* 2020;102:109305. doi: 10.1016/j.jbiomech.2019.07.049.
30. Schmid S, Connolly L, Moschini G, Meier ML, Senteler M. Skin marker-based subject-specific spinal alignment modeling: A feasibility study. *J Biomech.* 2022;137:111102. doi: 10.1016/j.jbiomech.2022.111102.
31. Salmingo R, Tadano S, Fujisaki K, Abe Y, Ito M. Corrective force analysis for scoliosis from implant rod deformation. *Clin Biomech (Bristol, Avon).* 2012; 27(6):545-50. doi: 10.1016/j.clinbiomech.2012.01.004.
32. Wang X, Boyer L, Le Naveaux F, Schwend RM, Aubin C-E. How does differential rod contouring contribute to 3-dimensional correction and affect the bone-screw forces in adolescent idiopathic scoliosis instrumentation? *Clin Biomech (Bristol, Avon).* 2016;39:115-121. doi: 10.1016/j.clinbiomech.2016.10.002.
33. Kamal Z, Rouhi G, Arjmand N, Adeeb S. A stability-based model of a growing spine with adolescent idiopathic scoliosis: A combination of musculoskeletal and finite element approaches. *Med Eng Phys.* 2019;64:46-55. doi: 10.1016/j.medengphy.2018.12.015.
34. Skov ST, Li H, Hansen ES, et al. New growth rod concept provides three dimensional correction, spinal growth, and preserved pulmonary function in early-onset scoliosis. *Int Orthop.* 2020; 44(9):1773-1783. doi: 10.1007/s00264-020-04604-y.
35. Lechner R, Putzer D, Dammerer D, Liebensteiner M, Bach C, Thaler M. Comparison of two-and three-dimensional measurement of the Cobb angle in scoliosis. *Int Orthop.* 2017; 41(5):957-962. doi: 10.1007/s00264-016-3359-0.